Engineering Fracture Mechanics 178 (2017) 457–476

Contents lists available at ScienceDirect

Engineering Fracture Mechanics

journal homepage: www.elsevier.com/locate/engfracmech

A new specimen for mixed mode-I/II fracture tests: Modeling, experiments and criteria development

Oğuzhan Demir [a,b], Ali O. Ayhan [a,*], Sedat İriç [a]

[a] Department of Mechanical Engineering, Sakarya University, 54187 Sakarya, Turkey
[b] Department of Mechanical and Manufacturing Engineering, Bilecik Şeyh Edebali University, 11210 Bilecik, Turkey

ARTICLE INFO

Article history:
Received 22 June 2016
Received in revised form 25 January 2017
Accepted 22 February 2017
Available online 8 March 2017

Keywords:
Mixed mode fracture
Fracture test
Stress intensity factor
T-specimen

ABSTRACT

Details related to modeling and experimental analyses for a new type of specimen, which is proposed to be used for mixed mode-I/II fracture tests, are presented. The specimen is similar to a T-shape and requires less material compared to some other specimens existing in the literature. Specimens are made from Al 7075-T651 rolled plates in the L-T rolling direction (crack plane is perpendicular to the rolling direction). Stresses in the loading apparatus and distributions of mixed mode stress intensity factors (SIFs) on the specimen are determined for all load mixity cases and comparisons are made for different specimen types. To check the validity of results obtained from numerical and experimental analyses of the T-specimen, similar studies are also performed for a different type of mixed mode-I/II compact tension shear (CTS) specimen. The results show that the T-specimen along with a suitable loading apparatus can be used for mixed mode-I/II fracture tests. Critical fracture loads obtained for the specimens are compared with criteria existing in the literature for mixed mode-I/II fracture conditions. It is found that most existing criteria start deviating from the experimental measurements for highly mixed mode loading conditions. Therefore, using all data obtained from numerical and experimental analyses, first an improved empirical mixed mode-I/II fracture criterion is proposed, which is followed by application on the T-specimen experiments for validation. The improved criterion shows excellent agreement with the experimental measurements. Thus, it is concluded that T-specimen and the newly developed criteria can be used for fracture problems with mixed mode-I/II loading conditions.

1. Introduction

Focusing initially on mode-I fracture problems, Fracture Mechanics concepts have been developed and applied on practical engineering problems successfully to assess safety and damage tolerance of structures over the past six decades. In many engineering problems faced with today, mixed mode fracture conditions are encountered due to different reasons; multi-axial and mixed mode loads, non-perpendicular orientation of crack surfaces with respect to uniaxial loading and different types and combinations of boundary conditions. Thus, thorough understanding and knowledge of mechanisms driving mixed mode fracture and crack growth conditions are necessary for accurate assessment of such conditions computationally and experimentally. Although initial studies on extension of an in-plane mixed mode crack can be traced back to five decades

* Corresponding author.
E-mail address: ayhan@sakarya.edu.tr (A.O. Ayhan).

http://dx.doi.org/10.1016/j.engfracmech.2017.02.019
0013-7944/

Nomenclature

ASTM	American Society for Testing and Materials
CT	compact tension
CTS	compact tension shear
f_j^k, g_j^k, h_j^k	mode I, mode II and mode III displacement components
Γ	local isoparametric coordinate
HSS	high speed steel
K_I, K_{II}, K_{III}	mode I, mode II and mode III stress intensity factors
K_I^i, K_{II}^i, K_{III}^i	nodal stress intensity factors
K_{eqv}	equivalent stress intensity factor range
Nj	regular finite element shape functions
P_{crt}	critical fracture load
$r(p)$	plastic zone size
SIF	stress intensity factor
θ	crack deflection angle
u_j^k, v_j^k, w_j^k	nodal displacements
ξ, η, ρ	local coordinates in the enriched element
Z_0	zeroing function

ago with Erdogan and Sih's work [1], especially in the last decades much more emphasis has been given to two- and three-dimensional mixed mode fracture and crack propagation problems in terms of detailed simulations and experiments, both of which are inseparable from each other.

In the literature, many studies can be found that deal with analyses of mixed mode fracture problems and experiments. Several stress or energy based fracture criteria are proposed so far to understand fracture mechanism of in plane mixed mode problems. Maximum tangential stress (MTS) [1], minimum strain energy density (SED) [2], maximum energy release rate (MERR) [3,4] and maximum tangential strain (MTSN) [5] criteria are some of the most common theoretical criteria used in fracture and crack propagation analyses for mixed mode-I/II fracture problems. Pook [6], Richard [7–9] and Tanaka [10] also proposed different fracture criteria by defining equivalent SIF equations. Much further details of in plane mixed mode fracture criteria can be found in [11,12]. Numerous numerical and experimental analyses were also performed in the literature by using different specimen types such as, disk type specimen [13–15], three or four-point bend specimens [16,17], rectangular specimen with an angled edge or central crack [18,19], Arcan specimen [20] and compact tension shear specimen, [21,22] designed for mixed mode loading cases to evaluate the criteria mentioned above. CTS (compact tension shear) specimen is one of the most commonly used specimens by researchers [7–9,21–30] with different sizes used in numerical and experimental analyses for mixed mode cases.

To be able to assess mixed mode fracture conditions, knowledge of both mixed mode crack driving forces under given loading, i.e., SIFs, and material response, i.e., fracture toughness, to mixed mode loading is needed. The material response to mixed mode fracture must be identified in a systematic and accurate way such that well-accepted standard fracture test requirements established for mode-I conditions are not violated. In addition, performing these tests with equipment and specimens that are as compact as possible and without sacrificing from these requirements is very desired to not only reduce test load levels but also to dispose less specimen material for each test.

The aim of this study is to propose a new specimen, named as T-specimen, which requires less material and lower fracture loads to failure compared to some other specimens existing in the literature used for mixed mode-I/II fracture tests. In what follows, first, modeling of the T-specimen for in plane mixed mode fracture tests is given including design analyses to determine stresses and deformations on the specimen and the apparatus. Based on results of the design analyses, the specimen dimensions are finalized. Then, systematic and detailed three-dimensional fracture analyses are performed to determine SIF distributions along the crack front in the specimen for different mode mixity ratios and comparisons are also made for different specimen types. In terms of mixed mode SIFs for different loading angles and fracture loads, T-specimen comparisons with CTS specimens having different dimensions are presented. Finally, the results obtained from numerical and experimental analyses are compared with related criteria existing in the literature. It is observed that most existing criteria start deviating from the experimental measurements for highly mode-II conditions. Therefore, new and improved criteria with consistent terms for equivalent SIF and crack deflection angle are proposed. This is done by making use of the analysis and experimental results from a different specimen to come up with a criterion, applying the criterion to the results of the T-specimen and refinement of the criterion by making use of all the data including from the T-specimen.

In previous papers [31,32], similar studies consisting of detailed finite element models including fracture submodels, description of the test procedure and the corresponding experimental results were performed for CTS specimen proposed by Richard [21,22] and a new empirical mixed mode-I/II criteria for onset of fracture and crack deflection angle were proposed. However, the developed empirical criteria had included inconsistent terms, i.e., not having the same units, in the

equations. Therefore, using the results of analyses and experiments, improved empirical criteria with consistent terms, i.e., with same units, in terms of fracture and crack deflection angle are developed in this paper.

2. Modeling of T-specimen for mode-I/II fracture tests

In this section, modeling details of T-specimen for in-plane mixed mode fracture tests are provided. First, specimen concept and geometry features are described, which is followed by detailed finite element analyses of the specimen for different mixed mode loading conditions to monitor stresses and plastic zone sizes at the crack tip. Based on the detailed finite element results, specimen geometry is finalized and test assembly is analyzed as a whole, including loading apparatus, clevises, pins and the contact mechanics between different parts of the assembly.

2.1. Specimen concept

In this subsection, the motivations for proposing a new mixed mode specimen and basic features about the T-specimen are presented. In Fig. 1, proportions of the T-specimen and its loading apparatus are shown. As can be seen from this figure, the specimen contains four loading holes to prevent free-rotation under mixed mode loads and that the specimen is attached to the loading apparatus through these four holes attached to the mixed mode loading apparatus. In Fig. 1b, for clarity only the bottom lower apparatus, which contains loading holes that are 15° apart from each other, is shown.

2.2. Design analyses of the T-specimen

Using the above described specimen concept, detailed preliminary stress and fracture analyses are performed to obtain an optimum specimen geometry with different specimen dimensions. ANSYS™ [33] is used to generate finite element models and perform stress analyses. For fracture analyses, FRAC3D solver, a general-purpose finite element based 3-D fracture analysis program [34,35] employing enriched crack tip elements to compute the SIFs, is used. The enriched finite elements do not require special mesh near crack front and SIFs are directly solved for at the same time as nodal displacements without any post-processing effort. Details of the enriched finite elements are given in the following section. Minimum-thickness calculations are also performed to make sure that plastic zone size is smaller than 1/50 of the specimen thickness for different mode mixity ratios, which is a condition to ensure plane strain fracture toughness test. From the results of fracture analyses, equivalent SIFs on the crack front are calculated using existing in-plane mixed mode fracture criteria. In the following preliminary design analyses, the main goal is to determine appropriate specimen dimensions to satisfy size requirements, taking into account plastic zone sizes under mixed mode loading conditions. Therefore, in these analyses, a simple statics approach is applied on the specimen without mixed mode loading apparatus, pins and contact mechanics to save time. Boundary conditions and loads are applied to only specimen and loading holes and analyses are performed by taking into consideration the case with maximum fracture loads, i.e., pure mode-II, $\theta = 90°$. For the specimen material of Al 7075-T651 aluminum alloy, Young's modulus and Poisson's ratio are 70 GPa and 0.33, respectively. Table 1 summarizes proportions and analyses results of the specimen used in detailed preliminary stress and fracture analyses. First, the outer dimensions of the T-specimen are approximated to those of the standard compact tension (CT) specimen. By taking thickness of the specimen as 25 mm and the loading to be 10 kN, stress and fracture analyses are, then, performed on specimens with different short-edge lengths and specimen dimensions (Model No.: M-1 and M-2 in Table 1). Using these results and an existing failure criterion from the literature, i.e., Richard [7–9], estimated fracture loads are also computed for these two

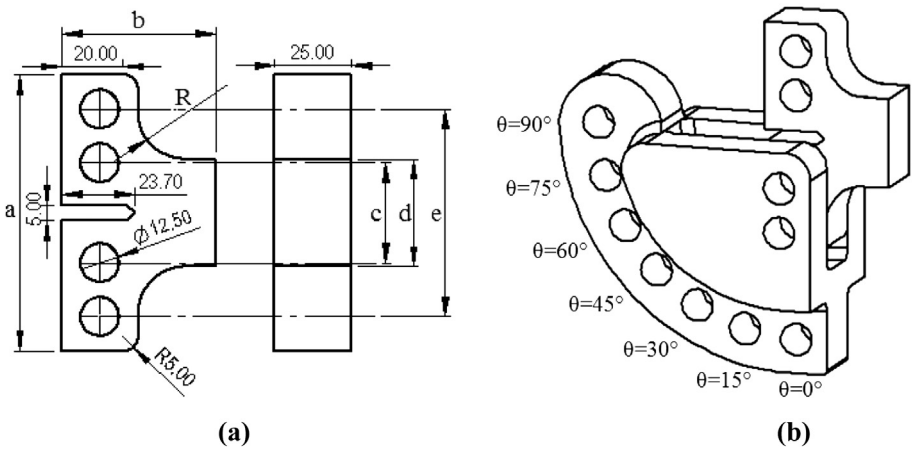

Fig. 1. (a) T-specimen proportions and (b) overall views of mixed mode loading apparatus.

Table 1
Specimen proportions used in design analyses and results of fracture analyses (applied load-10 kN and the specimen thickness-25 mm).

Model no.	Dimensions (mm)						SIFs ($MPa^a\ m^{1/2}$)				Critical load (kN)
	a	b	c	d	e	R	K_I	K_{II}	K_{III}[a]	K_{eqv}	P_{crt}
M-1	90	62.5	27.5	60	67.5	5	0.00	2.73	1.30	3.11	93.4
M-2	90	62.5	27.5	50	67.5	5	0.00	3.03	1.45	3.44	84.2
M-3	90	50	32.5	35	67.5	10	0.00	3.65	1.40	4.23	68.6
M-4	100	50	42.5	35	77.5	15	0.00	3.10	1.33	3.59	80.8
M-5	105	50	47.5	35	82.5	20	0.00	2.41	1.11	2.80	103.7

[a] K_{III} SIF values represent the edge values of crack front, since $K_{III} = 0$ at the center of the crack front.

cases and are included in the table. It is seen that although the required critical fracture load decreases with decreasing short-edge length of the specimen, still somewhat high fracture loads are expected for both designs considering load capabilities of most universal testing machines.

One of the important characteristics of the mixed mode SIF distributions on the crack front is the existence of the mode-III SIF along the crack front, although the loading is pure mode-II. A closer assessment of the finite element results yields that the generation and variation of the mode-III SIF is due to the Poisson's ratio of the material. To demonstrate this effect, the specimen is loaded with $\theta = 45°$, i.e., mode-I/II loading, and the resulting mixed mode SIF distributions are plotted in Fig. 2a. It is seen from the figure that mode-I and mode-II SIFs are nearly constant along the crack front and that, although there is no mode-III external loading, mode-III SIF varies linearly. To substantiate this behavior on mode-III SIF, top views of the borders of upper and lower crack surfaces are plotted before and after deformation, i.e., load application, in Fig. 2b. Owing to the applied mixed mode load, upper crack surface is under compressive and lower crack surface is exposed to tensile stress along the crack length direction. Thus, transverse expansion and contraction occur on the upper and lower crack surfaces, respectively. Consequently, this relative deformation between the upper and lower crack surfaces in the very near vicinity of the out-of-plane crack front causes positive and negative tearing mode SIFs on the two sides of the specimen, and this relative difference in the out-of-plane direction is zero at the specimen's central plane. For this reason, mode-III SIF values are zero at the center of the crack front. Buchholz et al. [36] also observed mode III effect locally along the crack front under in-plane mixed mode loading and noted the effect of Poisson's ratio on this behavior. Therefore, it is anticipated that mode-III SIF plays a significant role for highly mode-II conditions in mixed mode-I/II fracture experiments. To fracture the specimen for highly mode-II conditions, the required loads levels and plastic zone size increase. As a consequence, to provide small scale yielding conditions under LEFM (Linear Elastic Fracture Mechanics) rules, the required specimen thickness also increases.

Additional many analyses are also performed by changing specimen width, height, the distance between loading holes and the vertical positions of loading holes with respect to the crack plane. As a result of these analyses, specimen width and short edge length are decided to be 50 mm and 35 mm, respectively. Next, effects of long vertical edge length and the distance between loading holes on the SIFs and plastic zone sizes are investigated (Model No.: M-3, M-4 and M-5 in Table 1). In Fig. 3, resulting plastic zone sizes of specimens, M-3, M-4 and M-5, and equivalent stress distributions around the crack tip based on the yield strength, which is assumed as 460 MPa, are given. In this figure, the gray regions represent the extents of zones having higher stresses than the yield strength. As shown in the figure, having measured the plastic zone sizes, the required minimum thickness values are calculated from the measured plastic zone sizes and the predicted critical fracture load using existing fracture criteria [7–9]. As can be seen from the results, required critical fracture load and, accordingly, minimum thickness value increases with increasing the distance between loading holes to the crack front. Based on

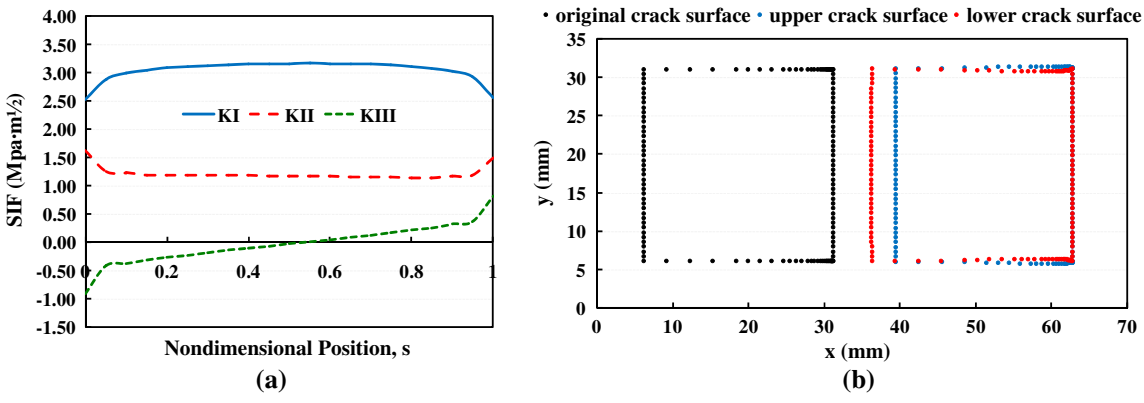

Fig. 2. (a) Variation of SIFs along the crack front and (b) original crack surface boundaries before and after application of the loads - 45° loading angle.

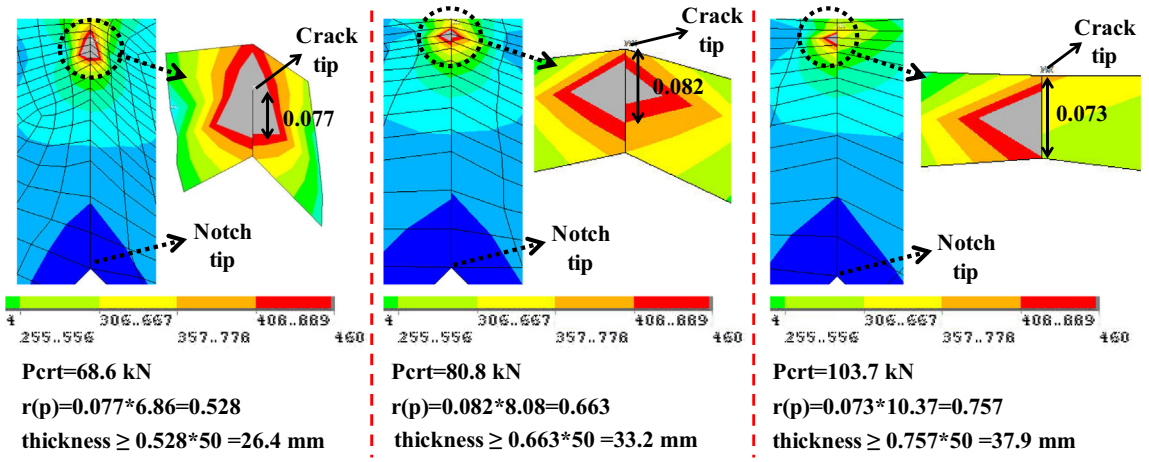

Fig. 3. Plastic zone size and minimum thickness values of specimens, M-3, M-4 and M-5 respectively.

these results, the first option is suitable with a minimum thickness of 26.4 mm. However, since the experiments performed in this study do not involve pure mode-II, the thickness is chosen to be 25 mm. Consequently, final sizes of the T-specimen, M-3, are determined as an optimum specimen geometry. Thus, in this study, a T-specimen which has smaller dimensions requiring less material and lower load levels for the same thickness compared to some other specimens existing in the literature is proposed for in-plane mixed mode fracture tests. In what follows, all details of the analysis procedure for the test assembly and the corresponding results are presented.

2.3. Analyses of the test assembly

In this section, details and results for the analyses of the whole assembly are presented. Mixed mode loading apparatus are designed to allow the loading axis to pass through the mid-point of the loading holes under different loading angles (0°, 15°, 30°, 45°, 60°, 75°, 90°). The steps involved in the analysis of the whole assembly are shown in Fig. 4. Modeling and the solution of the problem involving the whole assembly, i.e., loading devices, pins and the specimen, with contact mechanics are performed using ANSYS™. To simulate the real conditions as in the experiments, contacts are defined between the contact surfaces of the loading devices, pins and specimen (Fig. 4). Also, to simulate the actual conditions in the tensile test machine, boundary conditions are defined such that the surface nodes of the bottom loading clevis are constrained in all directions and

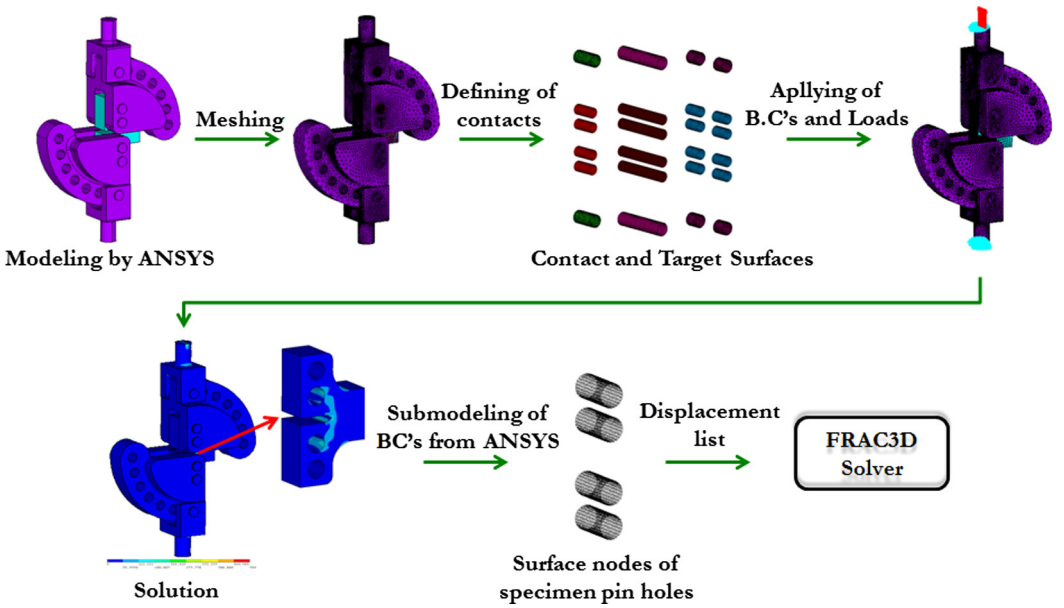

Fig. 4. Process map of the overall stress analysis procedure.

those of the upper loading clevis are allowed to move along the loading axis only, i.e., y-direction. Load is applied on the upper loading clevis in the vertical direction. Having obtained the overall solution using ANSYS™, displacements are taken from nodes of the loading hole surfaces of the specimen by using submodeling. Then these displacements are applied on the specimen model, and three-dimensional fracture analyses are performed using FRAC3D, a standalone finite element program employing enriched finite elements, to calculate the resulting SIFs. In the next section, results of the three-dimensional fracture analyses are given.

3. Three-Dimensional fracture analyses of the T-specimen

Having performed detailed stress analyses for the specimen and the test assembly to finalize their geometric details, three-dimensional fracture analyses under different in-plane mixed mode conditions are performed in this section. In what follows, analysis method is described first. In the following sub-sections, distributions of mixed mode three-dimensional SIFs for different mixed mode conditions and comparisons with other specimen types are given.

3.1. Analysis method

In this sub-section, the analysis method employed for computation of three-dimensional SIFs using enriched finite elements [35,37,38] is briefly described. As shown in Fig. 5, enriched elements are those elements that touch the crack front, whereas those elements located between enriched elements and regular finite elements are classified as transition elements.

In Fig. 6, a schematic of 20-noded hexahedral enriched crack tip element on an arbitrarily oriented crack front is shown. For an integration point at ξ, η and ρ, element local coordinates, three-dimensional displacement fields of enriched and transition elements are given by [39],

$$\begin{aligned} u(\xi,\eta,\rho) = {} & \sum_{j=1}^{m} N_j(\xi,\eta,\rho)u_j + Z_0(\xi,\eta,\rho)\left(f_u(\xi,\eta,\rho) - \sum_{j=1}^{m} N_j(\xi,\eta,\rho)f_{uj}\right)\left(\sum_{i=1}^{ntip} N_i(\Gamma)K_I^i\right) \\ & + Z_0(\xi,\eta,\rho)\left(g_u(\xi,\eta,\rho) - \sum_{j=1}^{m} N_j(\xi,\eta,\rho)g_{uj}\right)\left(\sum_{i=1}^{ntip} N_i(\Gamma)K_{II}^i\right) \\ & + Z_0(\xi,\eta,\rho)\left(h_u(\xi,\eta,\rho) - \sum_{j=1}^{m} N_j(\xi,\eta,\rho)h_{uj}\right)\left(\sum_{i=1}^{ntip} N_i(\Gamma)K_{III}^i\right) \end{aligned} \tag{1}$$

$$\begin{aligned} v(\xi,\eta,\rho) = {} & \sum_{j=1}^{m} N_j(\xi,\eta,\rho)v_j + Z_0(\xi,\eta,\rho)\left(f_v(\xi,\eta,\rho) - \sum_{j=1}^{m} N_j(\xi,\eta,\rho)f_{vj}\right)\left(\sum_{i=1}^{ntip} N_i(\Gamma)K_I^i\right) \\ & + Z_0(\xi,\eta,\rho)\left(g_v(\xi,\eta,\rho) - \sum_{j=1}^{m} N_j(\xi,\eta,\rho)g_{vj}\right)\left(\sum_{i=1}^{ntip} N_i(\Gamma)K_{II}^i\right) \\ & + Z_0(\xi,\eta,\rho)\left(h_v(\xi,\eta,\rho) - \sum_{j=1}^{m} N_j(\xi,\eta,\rho)h_{vj}\right)\left(\sum_{i=1}^{ntip} N_i(\Gamma)K_{III}^i\right) \end{aligned} \tag{2}$$

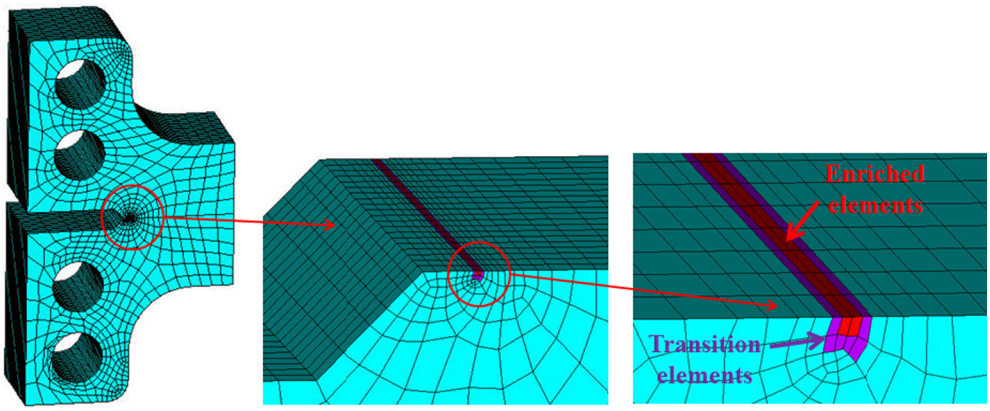

Fig. 5. T-specimen fracture finite element model, the enriched and transition elements.

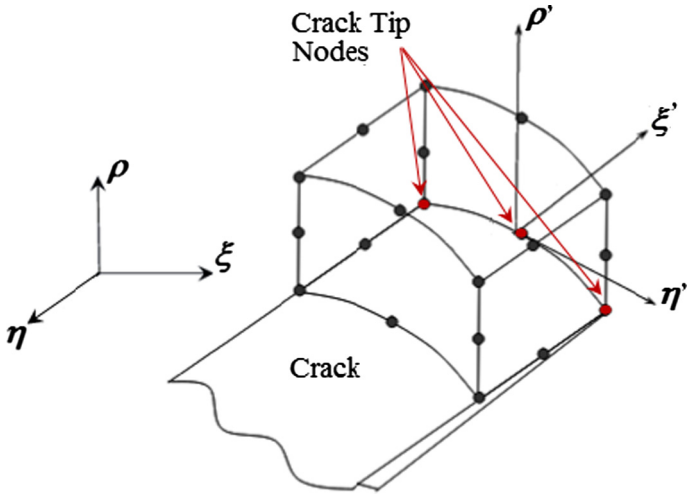

Fig. 6. Schematic of a 20-noded hexahedral enriched crack tip element on an arbitrarily oriented 3-D crack front.

$$
\begin{aligned}
w(\xi,\eta,\rho) = \sum_{j=1}^{m} N_j(\xi,\eta,\rho) w_j &+ Z_0(\xi,\eta,\rho)\left(f_w(\xi,\eta,\rho) - \sum_{j=1}^{m} N_j(\xi,\eta,\rho) f_{wj}\right)\left(\sum_{i=1}^{ntip} N_i(\Gamma) K_I^i\right) \\
&+ Z_0(\xi,\eta,\rho)\left(g_w(\xi,\eta,\rho) - \sum_{j=1}^{m} N_j(\xi,\eta,\rho) g_{wj}\right)\left(\sum_{i=1}^{ntip} N_i(\Gamma) K_{II}^i\right) \\
&+ Z_0(\xi,\eta,\rho)\left(h_w(\xi,\eta,\rho) - \sum_{j=1}^{m} N_j(\xi,\eta,\rho) h_{wj}\right)\left(\sum_{i=1}^{ntip} N_i(\Gamma) K_{III}^i\right)
\end{aligned} \tag{3}
$$

In (1)–(3), N_j are the regular element shape functions, u_j, v_j and w_j are the nodal displacements, Z_0 is a zeroing function that varies between 0 and 1. It is 1 for all enriched elements touching the crack front nodes. For the transition elements that surround crack front enriched elements and located between the enriched elements and regular finite elements this function takes a value of 0 at nodes shared by regular elements, a value of 1 at nodes shared by crack tip elements and contains up-to tri-linear variation between these two values for integration points inside the element. f_u, g_u, h_u, f_v, g_v, h_v, f_w, g_w and h_w are the analytically known terms from asymptotic crack tip displacement functions for mode I, mode II and mode III displacement components. K_I^i, K_{II}^i and K_{III}^i are the unknown nodal SIFs at the ith crack front node, and $\left(\sum_{i=1}^{ntip} N_i(\Gamma) K_{I,II,III}^i\right)$ represents the variation of the SIFs along the crack front on the element edge. For a model with quadratic elements, $ntip = 3$. As such, the variation of SIFs along the whole crack front is defined in a piecewise quadratic fashion by making use of the piecewise variations on all elements along the crack front. As can be seen from Eqs. (1)–(3), unknown SIFs on the crack front are included in the displacement fields of the crack tip elements, which are solved at the same as the nodal displacements during the solution of simultaneous linear finite element equations. Much further details and validations of the three-dimensional enriched elements for a variety of single-crack applications can be found in [35,37–39].

3.2. Mixed mode SIFs

Mixed mode I/II fracture analyses are performed for the 25 mm-thick T-specimen with a crack length of 25 mm under different loading angles (0°, 15°, 30°, 45°, 60°, 75°, 90°). 10 kN tensile load is applied for all analyses. Distributions of mixed mode three-dimensional SIFs for all loading conditions are given in Fig. 7. It is seen that, as expected, K_{II} and K_{III} increase with increasing loading angle while K_I decreases. Since fatigue pre-crack lengths measured after experiments are not always 25 mm and that one needs to have the SIF values for the exact crack length observed before fracture during the test, analyses are also performed for 26 and 27 mm crack lengths. Thus, using results from all analyses with different crack lengths, K_I, K_{II} and K_{III} SIF values corresponding to actual crack length obtained from experiments can be calculated by interpolation. Table 2 summarizes SIFs obtained for the center point of the crack front for 25, 26 and 27 mm crack lengths under different loading angles. In the way the loads are applied, 0° loading angle case, i.e., mode-I loading, is different from the other cases. In this case, the load is applied to the upper and lower holes of the specimen using the axial loading clevis only. That is, the specimen is loaded from the outer two holes only. However, in the other loading cases, the load is applied on all four holes of the specimen through the mixed mode loading apparatus.

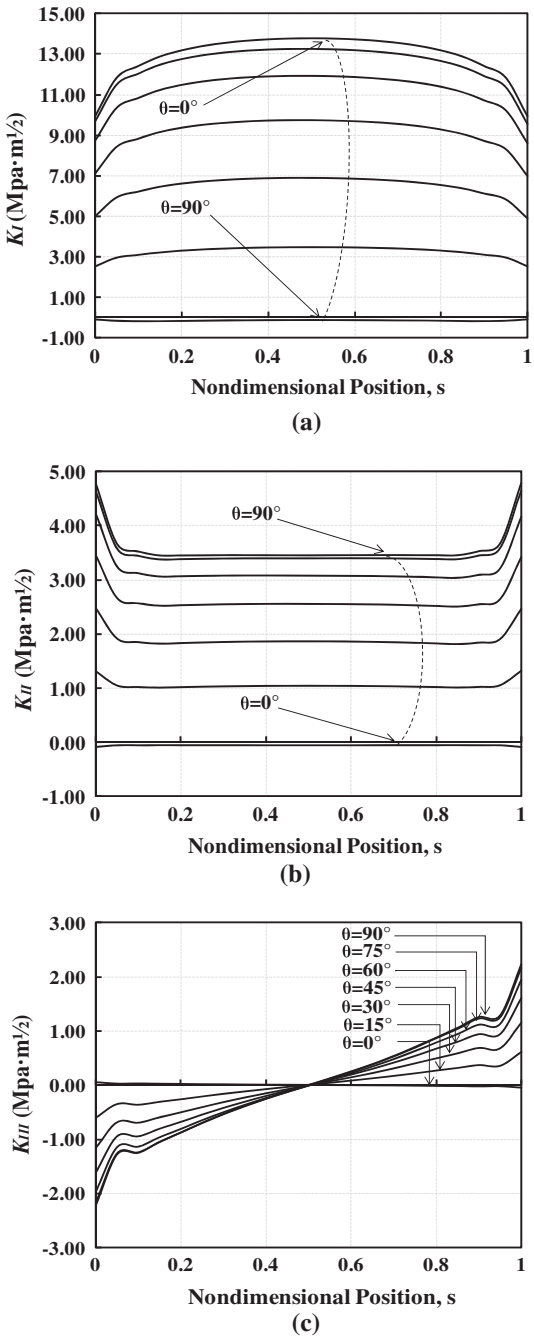

Fig. 7. Distributions of mixed mode three-dimensional SIFs for T-specimen under different mixed mode conditions (0°, 15°, 30°, 45°, 60°, 75°, 90°), (a) mode-I, (b) mode-II and (c) mode-III.

3.3. Comparisons with other specimen types

Up to now, various types of specimens have been proposed in the literature to understand the nature of fracture behavior of cracks exposed to in plane mixed mode loading. In this sub-section, comparisons of T-specimen with other specimen types in terms of mixed mode SIFs for a given loading angle are presented. CTS (compact tension shear) specimen (Fig. 8a), which is widely used in the literature and proposed by [21,22], its smaller version (Fig. 8b) studied by Zhao and Guo [29] and modified Arcan specimen, also called "butterfly specimen" (Fig. 8c), originally proposed by Arcan [40] and studied by [41,42], are evaluated in order to compare with the T-specimen (Fig. 8d). Loading devices suitable for these specimens are designed and

Table 2
K_I, K_{II} and K_{III} SIFs obtained from crack front center for 25, 26 and 27 mm crack lengths under different loading angles for 25 mm-thick T-specimen (M3).

Loading angle (°)	SIFs (MPa·m$^{1/2}$) (crack length-25 mm)			SIFs (MPa·m$^{1/2}$) (Crack length-26 mm)			SIFs (MPa·m$^{1/2}$) (Crack length-27 mm)		
	K_I	K_{II}	K_{III}	K_I	K_{II}	K_{III}	K_I	K_{II}	K_{III}
0	13.80	0.00	0.00	14.15	0.00	0.00	–	–	–
15	13.27	1.04	0.00	13.96	1.01	0.00	14.26	1.08	0.00
30	11.93	1.87	0.00	12.64	1.81	0.00	12.90	1.96	0.00
45	9.76	2.56	0.00	10.42	2.48	0.00	10.62	2.69	0.00
60	6.88	3.08	0.00	7.46	2.99	0.00	7.59	3.25	0.00
75	3.50	3.39	0.00	3.73	3.66	0.00	4.04	3.58	0.00
90	−0.12	3.45	0.00	–	–	–	–	–	–

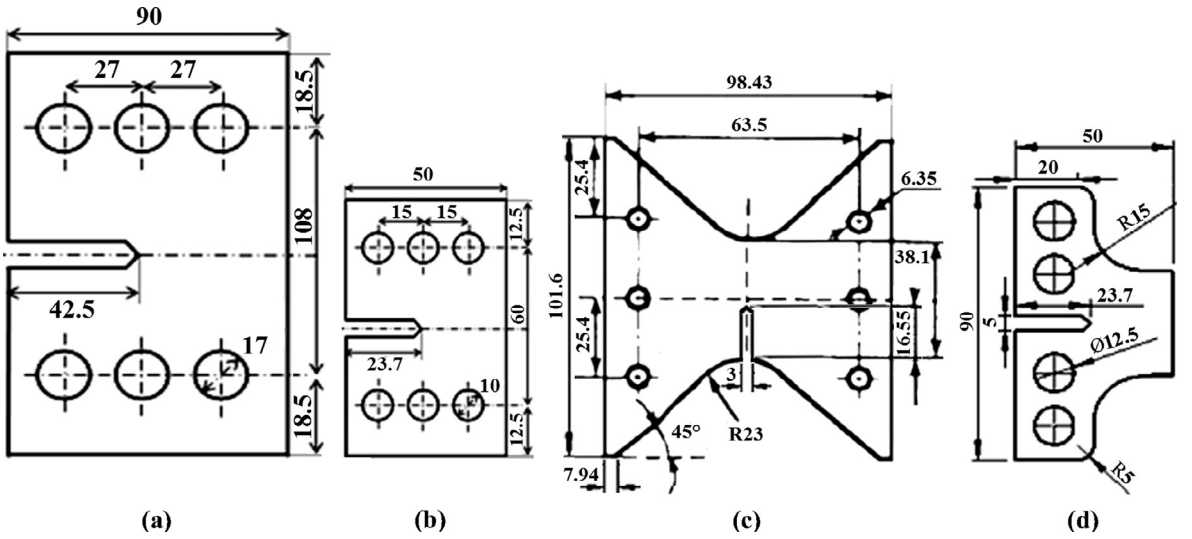

Fig. 8. The geometries and dimensions of different specimens, (a) Richard's specimen [19,20], (b) Zhao and Guo's specimen [32], (c) Modified Arcan's specimen [44,45] and (d) T-specimen.

modeled together with the specimens, which all had a thickness of 25 mm. Fracture analyses are also performed for these configurations with different loading angles. Distributions of mixed mode three-dimensional SIFs along crack front under 10 kN mixed-mode loading case (45°) for all specimens are shown in Fig. 9. It can be clearly seen from the figure that, compared to results of the other specimens, higher SIF values are obtained for the T-specimen for all three modes under the same external loading conditions.

The specimens compared above are different types of specimens used to determine fracture response of a material under different mixed mode loading conditions. Thus, for a given material test, generally numerous tests are performed to ensure repeatable and reproductable results, or in some cases, to obtain in statistical variation in material properties, which generally requires number of specimens produced in multiples of tens. Thus, minimization of material used and the necessary load capacity required for the tests is highly desired. To illustrate the importance of specimen sizes for total number of specimens that can be obtained from a fixed-size plate by machining operations, a comparison between Richard's and T-specimen in terms of saved machining time and material is given on a plate, 290 × 310 mm (Fig. 10). Number of Richard's and T-specimen obtained from this plate is 6 and 16, respectively. Moreover, from the outer dimensions of the two specimens, machining time expected for one Richard's specimen is about 1.7 times more compared to the T-specimen.

In addition to comparisons of analyses results and specimen dimensions, Richard's specimen together with its loading device is also manufactured for experimental work with their actual size and to be able to make comparisons between Richard's and T-specimen in terms of fracture loads. Results of stress and fracture analyses for 25 mm-thick Richard's specimen for all loading angles showed that required fracture loads are very high especially for highly mode-II conditions (60°, 75° and 90°). Therefore, as was done by Richard, 10 mm-thick CTS specimens are manufactured and used in the experimental studies. Fracture experiments are performed for the CTS specimen (10 mm-thick) and T-specimen (25 mm-thick) under different loading cases (0°, 15°, 30°, 45°, 60°, 75°). In Fig. 11, variations of fracture loads obtained from the experiments performed for CTS (10 mm-thick) and T-specimens (25 mm-thick) are given. It is seen that, although it is two and a half times thicker than the CTS specimen, lower fracture loads are obtained for the T-specimen under mixed mode loading conditions.

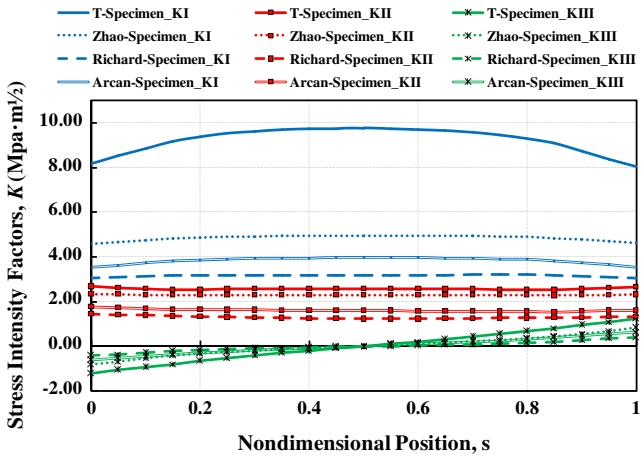

Fig. 9. Distributions of mixed mode three-dimensional SIFs under mixed mode loading (θ = 45°), applied load value is 10 kN and thickness is 25 mm for all specimens.

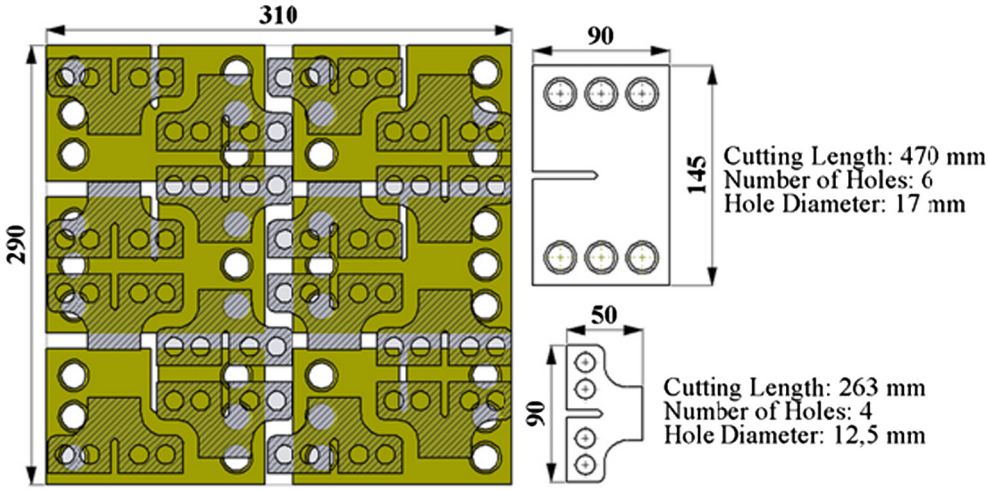

Fig. 10. A dimensional comparison between Richard's and T-specimen in terms of saving machining time and material.

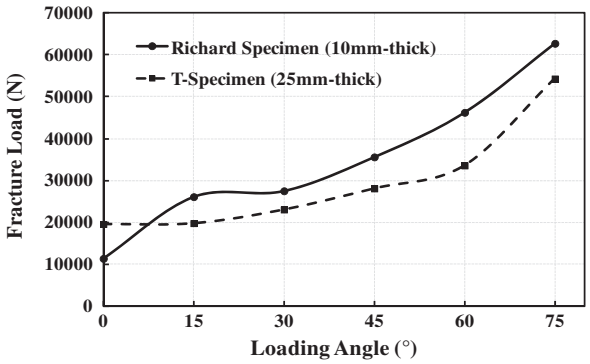

Fig. 11. Variations of fracture loads obtained from the experiments performed for Richard's and T-specimens under different loading angles (0°, 15°, 30°, 45°, 60°, 75°).

4. Fracture experiments using the T-specimen

In this section, experimental details of the T-specimen for in-plane mixed mode fracture tests are provided. First, experimental setup and used equipment are described, which is followed by validation of the finite element model using strain gage measurements and mode-I fracture toughness tests. Then, having presented results from all of the mixed mode tests performed, fracture loads are compared with some of the criteria existing in the literature.

4.1. Experimental setup

Mixed mode-I/II fracture experiments for the T-specimen are performed on a 100 kN "MTS 809" axial/torsional fatigue test machine. The specimens are made of Al 7075-T651 aluminum alloy and machined from rolled plates in the L-T rolling direction (crack plane is perpendicular to the rolling direction) and has a Young's modulus of 70 GPa, a Poisson's ratio of 0.33, and an initial yield stress of 460 MPa. The loading clevises are made of AISI 4140 steel and the loading pins are made of HSS steel. Modulus of elasticity and Poisson's ratio of the loading devices and pins are 200 GPa and 0.3 respectively.

In Fig. 12, overall views of the experimental set-up and the equipment used are shown. As seen from this figure, the test system consists of MTS test machine, T-specimen, the loading apparatus, the pins and a high-zoom camera used to monitor crack length and its propagation. 25 mm-thick T-specimens are used in the experiments.

Fatigue pre-cracking is performed under mode-I loading for all specimens according to ASTM E399 standard [43]. Pre-crack lengths of all specimens are determined as indicated in the standard (pre-crack Length $\geq$ 0.025 W or 1.3 mm whichever is larger). Also pre-crack load is determined according to the ASTM condition ($K_{max} \leq 0.8K_Q$). After generation of the pre-crack, tensile load is applied quasi-statically to the specimens by taking into account limitations in the standard that the specified rate of increase of the SIF ranges from 0.55 to 2.75 MPa $\sqrt{}$m/s, under different loading angles. Finally, load vs. displacement data are taken from the machine and critical fracture load is determined according to the options in the standard.

4.2. Validation studies using strain gages and mode-I fracture toughness tests

Strain gage application is performed to validate the results of simulations involving contact mechanics between loading devices, pins and the specimen. First, T-specimen with no crack is modeled and stress analysis is performed for test assembly as a whole, including mode-I loading apparatus, pins and the specimen under 10 kN load and 0° loading angle (mode-I loading) (Fig. 13(a)). ANSYS™ [33] is used to generate finite element models and perform stress analyses. After performing stress analysis, position and direction of strain gages are determined to be placed on the specimen according to distributions and directions of maximum principal stresses (Fig. 13(b)). Strain gauges are attached to the specimen with a special glue. In Fig. 14, overall and close-up views of the experimental set-up with strain gage applications are given. Load is applied to the specimen from 0 to 10 kN by an increment of 2 kN, then load is decreased from 10 kN to 0 by the same increment of 2 kN. The reason for applying the variable load is to ensure the load linearity and validate the sensitivity of strain gage measurements. The measured strain values and percent differences calculated from numerical and experimental analyses are given in Table 3. It is seen from this table that, with an average error rate of 1–3%, excellent agreement is obtained between experimental and numerical results.

Mode-I fracture toughness test is also performed to validate the results of stress and fracture analyses. From mode-I toughness testing of the T-specimen having 26.03 mm crack length and thickness of 24.87 mm, a fracture load of 19.60 kN is obtained. Load vs. displacement curve and fracture point are shown in Fig. 15. Considering the fracture toughness of the material (29 MPa $\sqrt{}$m), at the crack length observed in the experiment, the predicted fracture load is 21.01 kN. From another mode-I toughness testing having 27.57 mm crack length and thickness of 25.00 mm, experimental fracture load of 18.82 kN is obtained and 19.72 kN is predicted. Thus, it is concluded that good agreement is also found between experimental and numerical results of T-specimen with an error of approximately 6% in terms of mode-I fracture test.

4.3. Mixed mode fracture tests

In this subsection, results from the fracture tests of T-specimen are presented. In-plane mixed mode I/II fracture experiments are performed under different loading angles using pre-cracked T-specimens under mod-I conditions. Details of the experimental setup and used equipment are described in Section 4.1. Critical fracture loads are determined from load-displacement curves according to the ASTM E399 standard and crack deflection angles are measured from the fracture surfaces for all fractured specimens after the tests. In Fig. 16, overall view of fracture surfaces from broken samples are given. Consistent fracture surfaces and deflection angles are observed from the tests for all loading angles. Table 4 summarizes results of fracture tests for loading angles of 0°, 15°, 30°, 45°, 60° and 75°.

4.4. Comparisons of fracture loads with existing criteria

In order to validate the results of fracture analyses and experiments, fracture loads obtained from the tests are compared in this section with the existing criteria described earlier for in-plane mixed mode loading situations. First, for every loading

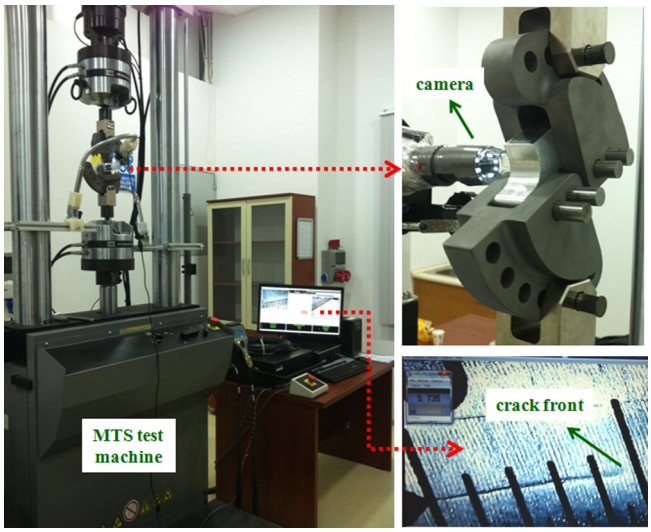

Fig. 12. Experimental set-up and MTS test machine.

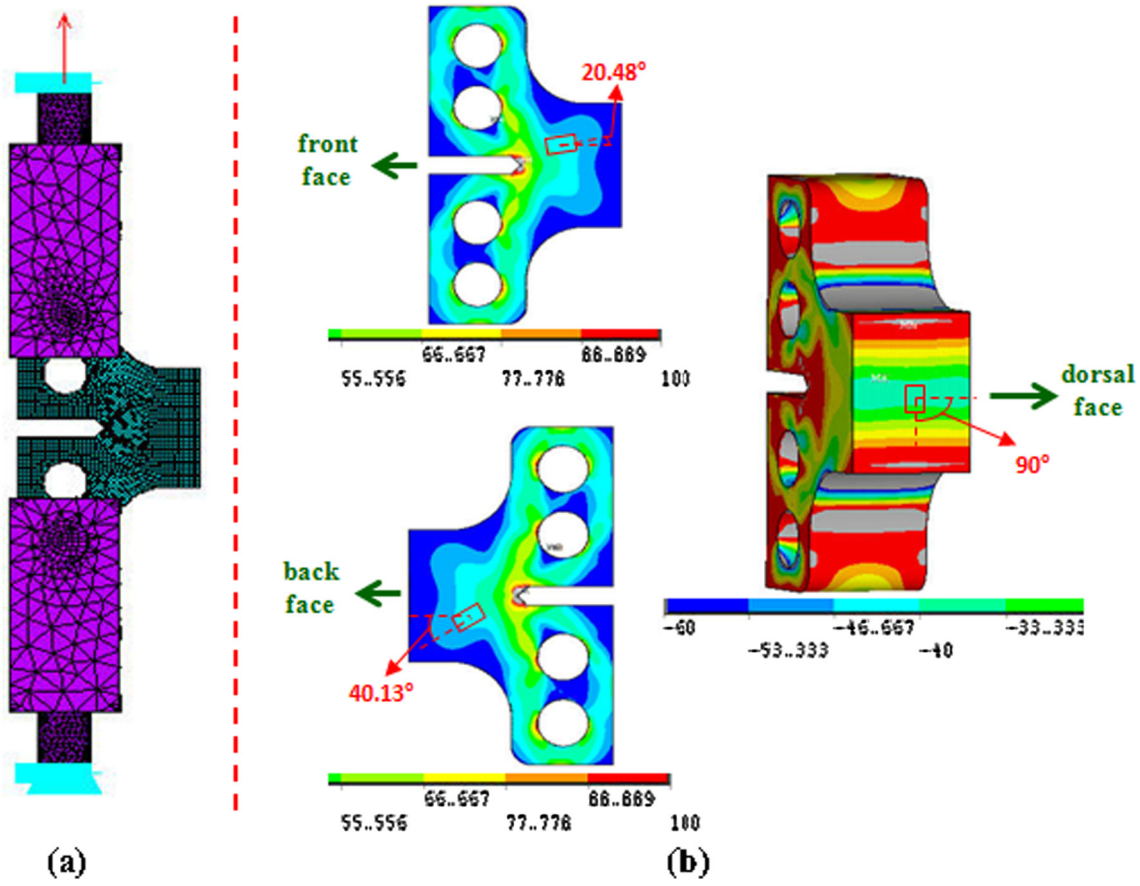

Fig. 13. Numerical analysis results for strain gage application of T-specimen, (a) Finite element model and (b) equivalent stress distributions.

cases SIFs (K_I and K_{II}) obtained from detailed finite element models of T-specimen are substituted into the equivalent SIF equations given by existing criteria. Then, critical fracture loads required to for equivalent SIF values to be equal to the fracture toughness (K_{IC}) value of the material according to different criteria are computed. The obtained results showed that, all

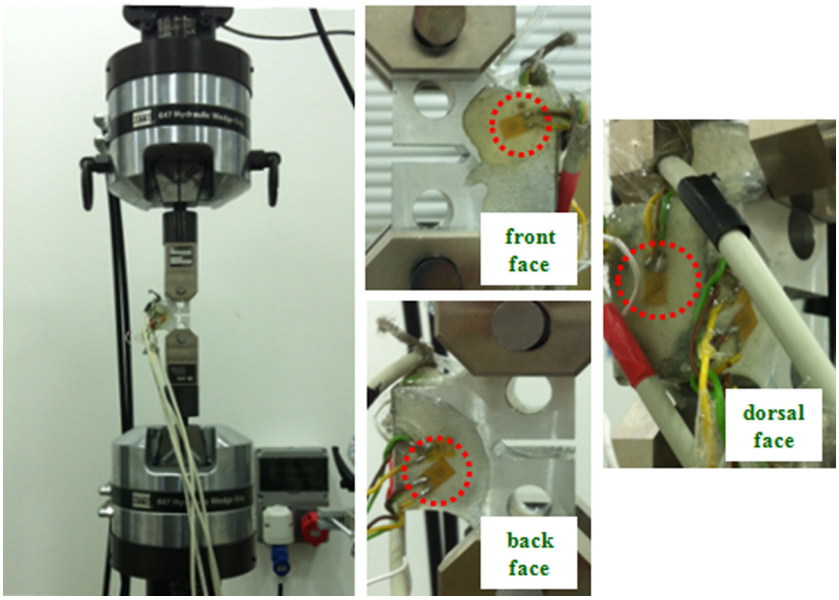

Fig. 14. Experimental set-up for strain gage application of T-specimen.

Table 3
Strain values measured and percent differences between numerical and experimental analyses.

Load (kN)	Front face	Diff. %	Dorsal face	Diff. %	Back face	Diff. %
Strain values measured from strain gages						
0–2	7.72E−05	0.84	−9.75E−05	2.72	7.03E−05	−9.77
0–4	1.54E−04	0.34	−1.99E−04	5.10	1.47E−04	−5.39
0–6	2.32E−04	0.86	−2.97E−04	4.21	2.21E−04	−5.43
0–8	3.06E−04	−0.12	−3.91E−04	3.00	3.00E−04	−3.79
0–10	3.79E−04	−0.91	−4.87E−04	2.54	3.80E−04	−2.54
Strain values calculated from ANSYS						
10	3.83E−04	−0.91	−4.74E−04	2.54	3.90E−04	−2.54

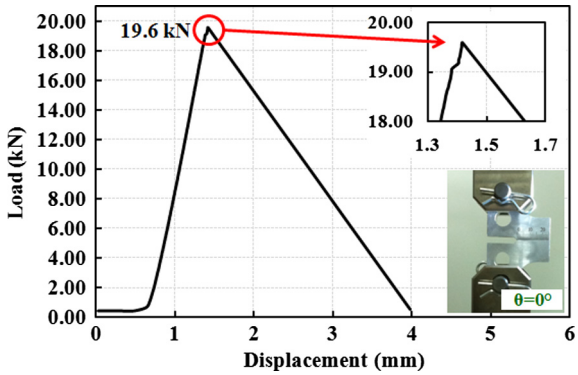

Fig. 15. Load-displacement curve of T-specimen for 0° loading angle during fracture toughness test.

criteria are in good agreement with the experimental results up to 60° loading angle. The predicted fracture loads by different criteria start to differ from the experimental measurements for cases with loading angles greater than 60°.

5. Development of new mode-I/II fracture criteria

In an effort to improve the aforementioned differences between predicted fracture loads by some of the existing criteria and the experimental measurements, details related to development of an improved mode-I/II fracture criteria are presented

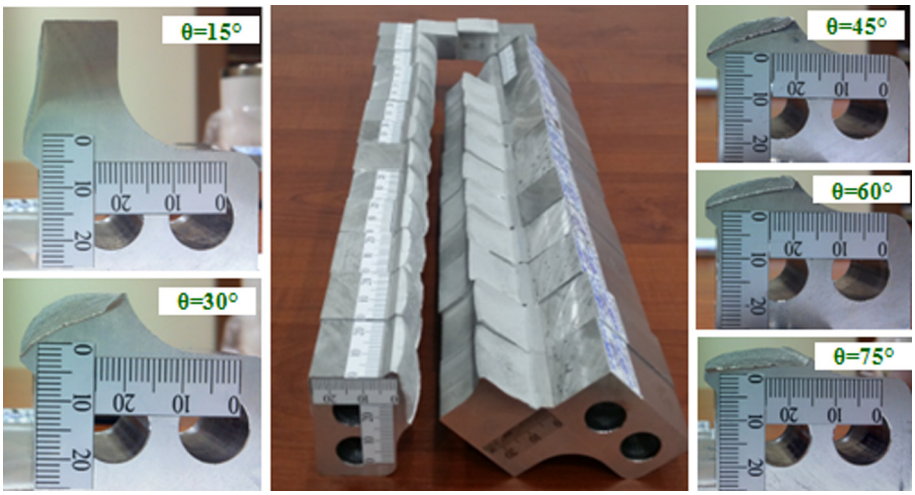

Fig. 16. Broken sample pictures and fracture surfaces of T-specimen for different loading angles.

Table 4
Experimental test results for 25 mm-thick T-specimen under different loading angles.

Specimen no.	Loading angle (°)	Thickness (mm)	Crack length (mm)	Experimental	
				Fracture load (kN)	Crack deflection angle (°)
T-01	0	24.87	26.03	19.60	0.0
T-02	0	25.00	27.57	18.82	0.0
T-03	15	25.00	26.93	19.80	−11.4
T-04	15	24.98	26.34	19.70	−11.1
T-05	30	24.98	26.21	23.07	−18.2
T-06	30	25.00	26.90	20.64	−19.8
T-07	45	25.00	25.24	28.09	−27.2
T-08	45	25.01	25.46	29.21	−26.9
T-09	60	24.96	27.13	33.59	−37.6
T-10	60	25.00	26.58	34.76	−42.4
T-11	75	25.03	26.89	54.31	−55.9
T-12	75	24.96	26.70	55.04	−62.0

in this section. First, current analysis and experimental results for a different specimen type, Richard's CTS specimen [21,22], are given. This is followed by development of a new mode-I/II criterion by using the numerical and experimental results of the CTS specimen and its application to the T-specimen test cases. Finally, by combining the analysis and experimental data for both CTS and the T-specimen, a further improved mixed mode-I/II fracture criteria are developed.

5.1. Analysis and experimental results from CTS specimen

CTS specimen has been studied very extensively by many scientists in the last two decades and well known to many researchers in fracture mechanics. To check the validity of results from the numerical and experimental analyses of the T-specimen, similar studies are also performed for the Richard's CTS specimen. Its detailed dimensions are given in Fig. 8a. Thus, first, finite element modeling and experimental studies are performed on this specimen both to gain confidence in the obtained results and identify any improvement needs for the mixed mode fracture criteria development. Similar analysis procedure to the one described in this study for the T-specimen is applied for CTS specimen. Detailed stress and fracture analyses are performed for all mode mixity cases using detailed three-dimensional finite element models, which include loading clevises, apparatus, pins, the specimen and contact mechanics between them. As is the case with the T-specimen, analyses are performed for 43.5, 45 and 47 mm crack lengths, since fatigue pre-crack lengths measured after experiments are not always at the same length. Using the additional analyses with different crack lengths, K_I, K_{II} and K_{III} SIF values corresponding to the actual crack length obtained from experiments can be calculated by interpolation. In a previous paper [31], details of the finite element models including fracture submodels, description of the test procedure and the corresponding experimental results were presented for the CTS specimen. In Table 5, K_I, K_{II} and K_{III} SIFs obtained from crack front center for 43.5, 45 and 47 mm crack lengths under different loading angles for 25 mm-thick CTS specimen are given. 0° loading case i.e. mode-I loading case, is obtained by applying the load to the upper and lower left holes of the specimen using the axial loading clevis only. However, load is applied to other holes of the specimen through the usage of the mixed-mode loading apparatus. Therefore, there is a high degree of change for K_I SIF values between 0° and 15° loading angles.

Table 5
K_I, K_{II} and K_{III} SIFs obtained from crack front center for 43.5, 45 and 47 mm crack lengths under different loading angles - 25 mm-thick CTS specimen [31,32].

Loading angle (°)	SIFs ($MPa^* m^{1/2}$) (crack length-43.5 mm)			SIFs ($MPa^* m^{1/2}$) (crack length-45.0 mm)			SIFs ($MPa^* m^{1/2}$) (crack length-47.0 mm)		
	K_I	K_{II}	K_{III}	K_I	K_{II}	K_{III}	K_I	K_{II}	K_{III}
0	8.78	0.00	0.00	9.13	0.00	0.00	9.59	0.00	0.00
15	4.37	0.32	0.00	4.60	0.46	0.00	5.13	0.43	0.00
30	3.91	0.65	0.00	3.91	0.82	0.00	4.59	0.94	0.00
45	3.16	0.94	0.00	3.17	1.18	0.00	3.74	1.35	0.00
60	2.23	1.15	0.00	2.20	1.48	0.00	2.63	1.72	0.00
75	1.05	1.30	0.00	1.10	1.67	0.00	1.31	1.94	0.00
90	–	–	–	0.00	1.73	–	–	–	–

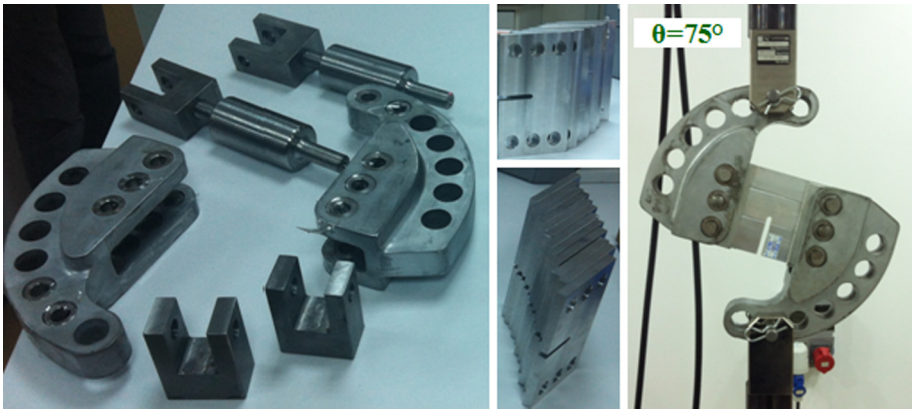

Fig. 17. Overall views of the experimental equipment used for testing CTS specimen [31,32].

In Fig. 17, overall views of the equipment used in fracture experiments of the CTS specimen with experimental set-up for 75° loading angle are shown. The same material, manufacturing and experimental test procedures are applied for CTS specimen as in the case of the T-specimen. Table 6 summarizes results of fracture tests of 10 mm-thick CTS specimen for 0°, 15°, 30°, 45°, 60°, 75° loading angles. In Fig. 18, overall views of fracture surfaces from broken samples are given. Consistent fracture surfaces and deflection angles are observed from the tests between different loading angles. In what follows, fracture loads obtained for CTS specimen are compared with some of the existing mode-I/II fracture criteria and are used to develop new and improved mode-I/II fracture criterion.

5.2. Development of new mode-I/II fracture criterion and application on T-Specimen

In an effort to develop an improved empirical in-plane mixed mode-I/II fracture criterion with consistent terms, mixed mode SIFs obtained from detailed fracture analyses of the CTS specimen and results from the fracture experiments for different mixed mode loading situations are used in a nonlinear regression analysis using Datafit™ [44]. The empirical mixed mode-I/II fracture criterion equation, i.e., equivalent SIF, is determined by performing nonlinear regression analyses using fracture loads measured from the experiments and mixed mode SIFs for all loading angles. This criterion proposes that when the equivalent SIF reaches the fracture toughness of the material under mode-I loading, unstable fracture occurs. Equivalent SIF (K_{eq}) in the developed criterion is defined by,

$$K_{eq} = \left(a \cdot K_I^4 + b \cdot K_{II}^4 + c \cdot K_I^2 \cdot K_{II}^2\right)^{1/4} \tag{4}$$

This equation is, first, developed by using only the CTS specimen data under 0°, 15°, 30°, 45°, 60° and 75° loading angles. Coefficients obtained from the nonlinear regression analyses for Eq. (4) are given in Table 7. Experimental loads and predicted fracture loads obtained from this developed criterion for the CTS specimen along with other existing criteria in the literature for different loading cases are given in Fig. 19. The developed criterion by using only the CTS specimen data is labeled in the graph as "Developed Criterion (1)". As can be seen in the figure, significant deviation occurs after 45° loading angle for Erdogan and Sih, Richard and Pook criteria and the difference increases with increasing loading angle. Tanaka criterion is in good agreement with the experimental results up to 60° loading angle but the criterion does not produce accurate result for 75° loading case. Critical load values predicted by developed criterion and obtained from experiments are in excellent agreement with an average error rate of 4.15% for different loading cases performed.

Table 6
Experimental test results for 10 mm-thick CTS specimen under different loading angles [31,32].

Specimen no.	Loading angle (°)	Thickness (mm)	Crack length (mm)	Experimental	
				Fracture load (kN)	Crack deflection angle (°)
CTS-01	0	10.00	46.50	11.38	0.0
CTS-02	15	10.07	46.07	26.11	−12.4
CTS-03	15	10.06	45.96	26.68	−12.6
CTS-04	30	9.60	45.08	27.52	−21.1
CTS-05	30	10.10	44.94	28.59	−20.7
CTS-06	30	10.20	45.03	29.57	−20.2
CTS-07	45	10.13	44.95	35.61	−31.2
CTS-08	45	10.17	44.75	33.00	−31.7
CTS-09	60	10.16	44.93	46.25	−43.1
CTS-10	60	10.15	45.22	46.90	−43.6
CTS-11	60	10.18	45.20	45.71	–
CTS-12	75	10.10	46.38	62.73	−61.5
CTS-13	75	10.14	45.24	68.07	−59.5

Fig. 18. Broken sample pictures and fracture surfaces of CTS-specimen for different loading angles performed [31,32].

Table 7
Coefficients of equivalent SIF equation developed using CTS specimen data.

a	b	c
0.9151	−0.2401	2.4070

In order to validate the so far developed criterion, which made use of only the CTS analysis and experimental data, Eq. (4) is also applied to the T-specimen test cases and the predicted and measured fracture loads are compared with each other. In Fig. 20, comparisons of the predicted fracture loads for the T-specimen using the developed criterion (labeled as "Developed criterion (1)") with other existing criteria in the literature and the experimental measurements for the T-specimen are given. Critical load values obtained from the developed criterion and experimental results are almost identical with an average error rate of 4.57% for different loading angles. Thus, the developed criterion, which so far is based only on the CTS data, is validated with direct application and comparison to T-specimen fracture results. Furthermore, the good comparison obtained between predictions and experimental measurements also proves that the proposed T-specimen is a valid and new type of specimen that can be used for mixed mode fracture toughness tests.

5.3. Refinement of new criterion using results from CTS and T-specimen

So far, the developed criterion by the CTS data only is validated against the T-specimen data. On the other hand, the T-specimen data also serves as an opportunity to additionally improve the criterion. Thus, by combining the analysis and experimental data for both CTS and the T-specimen a further improved equivalent SIF equation is developed in this subsection. 0° loading case data for CTS and T-specimens are also included. The form of equivalent SIF (K_{eq}) in the refined new criterion is the same as before and defined by,

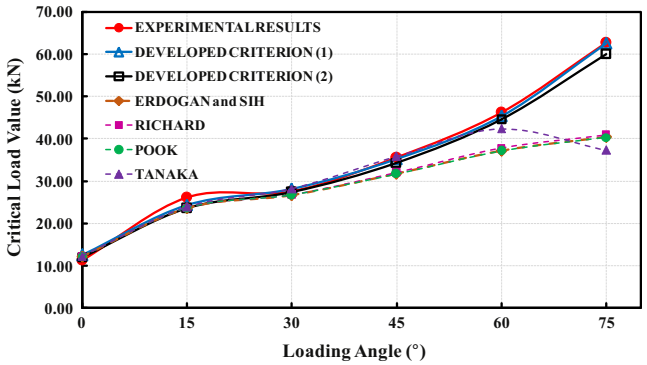

Fig. 19. Comparisons of experimental and predicted fracture loads for the CTS specimen using developed and existing fracture criteria.

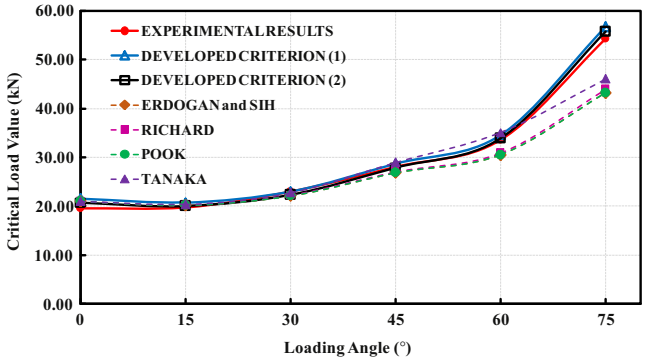

Fig. 20. Comparisons of experimental and predicted fracture loads for the T-specimen using developed and existing fracture criteria.

Table 8
Coefficients of new refined equivalent SIF equation.

d	e	f
1.0519	−0.0350	2.3056

$$K_{eq} = \left(\mathrm{d}\cdot K_I^4 + \mathrm{e}\cdot K_{II}^4 + \mathrm{f}\cdot K_I^2\cdot K_{II}^2\right)^{1/4} \tag{5}$$

Having used the described combined data from both types of specimens, coefficients in Eq. (5) are given in Table 8. Comparisons of predicted fracture loads obtained from this refined new criterion (labeled as "Developed criterion (2)") for the CTS specimen and T-specimen with other existing criteria in the literature and experimental fracture loads under different loading angles are given in Figs. 19 and 20, respectively. Critical load values of the refined new criterion and experimental results are good agreement with an average error rate of 4.67% for CTS and 2.92% for T-specimen under all loading angles including 0° loading angle.

Furthermore, experimental results are evaluated with existing fracture criteria in terms of crack deflection angles and a new improved empirical crack deflection angle equation for in-plane mixed mode loading is also proposed. For the determination of the equation, mixed mode SIFs obtained from detailed finite element models of CTS and T-specimen and crack deflection angles obtained from the experiments for all loading angles are used. Developed crack deflection angle equation is given in the following form,

$$\theta_0 = -\arccos\left(\frac{a\cdot K_{II}^2 + K_I\cdot\sqrt{K_I^2 + b\cdot K_{II}\cdot K_I} + c\cdot K_{II}\cdot K_I}{K_I^2 + d\cdot K_{II}^2}\right) \tag{6}$$

The coefficients of Eq. (6) obtained by using deflection angles from all of the CTS and T-specimens in the nonlinear regression analyses are given in Table 9. Variations of crack deflection angles based on different criteria with respect to K_{II}/K_I ratio and including experimental measurements are plotted in Fig. 21. The crack deflection angles obtained from the developed

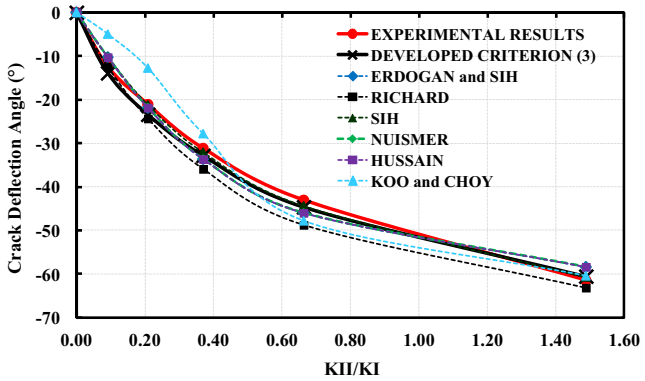

Fig. 21. Variations of crack deflection angles with respect to K_{II}/K_I ratio - CTS specimen.

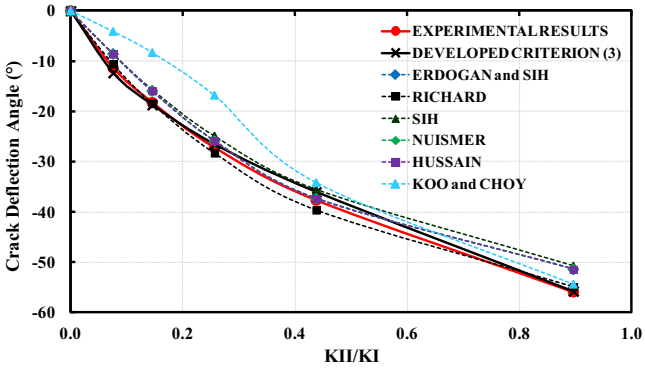

Fig. 22. Variations of crack deflection angles with respect to K_{II}/K_I ratio – T-specimen.

Table 9
Coefficients of new developed crack deflection angle equation using CTS and T-specimen data.

a	b	c	d
0.1723	5.1062	−2.7483	−1.1636

criterion and experimental results are almost identical with an average error of 6.58% for all loading angles. When compared with experimental results, crack deflection angles obtained from different criteria, except Koo and Choy criterion, show reasonably close agreement up to 45° loading angle, and start deviating from experiments for 60° and 75° loading cases. Similarly, variations of crack deflection angles as a function of K_{II}/K_I ratio are presented for T-specimen in Fig. 22. The predicted crack deflection angles are in good agreement with measured values with an average error of 4.59% considering all loading angles. It is seen from the figure that all of the criteria, except Koo and Choy criterion, have about the same and close tendency as the experimental results as is the case with the CTS specimen up to 45° loading angle. It is again seen that the difference between predicted and measured deflection angles increase for 60° and 75°loading angles. Finally, it is stated that the developed criterion for the crack deflection angle agrees well with the experimental measurements for both types of mixed mode specimens, namely the CTS specimen and the T-specimen.

6. Summary

In this study, details of modeling, mixed mode-I/II fracture analyses and experiments for a new type of specimen, named as T-specimen are presented. The specimen has smaller dimensions and requires less material compared to other specimen types used for the same purpose. The specimen is proposed with its loading device to be used for in-plane mixed mode fracture tests. The results and comparisons show that specimen structure and its configuration play a significant role to obtain higher mixed mode SIF values. This becomes more important especially for highly mode-II conditions in terms of fracture loads, since as mode mixity increases the fracture loads also increase. It is shown that the T-specimen, which requires less

material and lower fracture loads compared to some other specimens existing in the literature, can be used as a practical test configuration for mixed mode-I/II fracture investigations.

Detailed results from experimental studies of the T-specimen and their comparisons to predictions from the analyses using existing criteria in the literature are also presented in the study. To check the validity of the obtained results, they are compared with existing criteria in the literature for mixed mode-I/II fracture conditions. The results show that existing criteria yield reasonably close results to experiments for up to moderate levels of mode mixity in the loading. However, most existing criteria start deviating from the experimental measurements for highly mixed mode loading conditions. Therefore, using all data obtained from analyses and experiments of the CTS specimen, first an improved empirical mixed mode-I/II fracture criterion is proposed and for validity, it is applied to the newly proposed T-specimen. Refinement of the criterion for critical fracture loads and crack deflection angles are, then, performed by making use of all the data from both the CTS and the T-specimen. It is shown that the developed criteria for both onset of fracture and crack deflection angle under mixed mode conditions are in very good agreement with the experimental measurements. Thus, it is concluded that the newly developed criteria can also be used for fracture problems with mixed mode-I/II loading conditions.

Acknowledgement

The financial support by The Scientific and Technological Research Council of Turkey (TUBITAK) under Project Number: 113M407 for this study is gratefully acknowledged.

References

[1] Erdogan F, Sih GC. On the crack extension of plates under plane loading and transverse shear. J Basic Eng 1963;85:519–27.
[2] Sih GC. Strain energy density factor applied to mixed mode crack problems. Int J Fract 1974;10:305–21.
[3] Hussain MA, Pu SU, Underwood J. Strain energy release rate for a crack under combined mode I and II. ASTM STP 1974;560:2–28.
[4] Nuismer RJ. An energy release rate criterion for mixed mode fracture. Int J Fatigue 1975;11:245–50.
[5] Chang KJ. On the maximum strain criterion-a new approach to the angled crack problem. Eng Fract Mech 1981;14:107–24.
[6] Pook LP. The significance of mode I branch cracks for mixed mode fatigue crack growth threshold behaviour. In: Brown MW, Miller KJ, editors. Biaxial and multiaxial fatigue. London: Mechanical Engineering Publishing; 1989. p. 247–63.
[7] Sander M, Richard HA. Finite element analysis of fatigue crack growth with interspersed mode I and mixed mode overloads. Int J Fatigue 2005;27(8):905–13.
[8] Sander M, Richard HA. Experimental and numerical investigations on the influence of the loading direction on the fatigue crack growth. Int J Fatigue 2006;28:583–91.
[9] Richard HA, Schramm B, Schirmeisen N. Cracks on mixed mode loading-theories, experiments, simulations. Int J Fatigue 2014;62:93–103.
[10] Tanaka K. Fatigue crack propagation from a crack inclined to the cyclic tensile axis. Eng Fract Mech 1974;6:493–507.
[11] Qian J, Fatemi A. Mixed mode fatigue crack growth: a literature survey. Eng Fract Mech 1996;55(6):969–90.
[12] Rozumek D, Macha E. A survey of failure criteria and parameters in mixed-mode fatigue crack growth. Mater Sci 2009;45(2):190–210.
[13] Al Shayea NA. Crack propagation trajectories for rocks under mixed mode I-II fracture. Eng Geol 2005;81:84–97.
[14] Aliha MRM, Behbahani H, Fazaeli H, Rezaifar MH. Study of characteristic specification on mixed mode fracture toughness of asphalt mixtures. Constr Build Mater 2014;54:623–35.
[15] Akbardoost J, Rastin A. Comprehensive data for calculating the higher order terms of crack tip stress field in disk-type specimens under mixed mode loading. Theoret Appl Fract Mech 2015;76:75–90.
[16] Aliha MRM, Ayatollahi MR, Kharazi B. Numerical and experimental investigations of mixed mode fracture in granite using four-point-bend specimen. In: Boukharouba et al., editors. Damage and fracture mechanics: failure analysis of engineering materials and structures; 2009. p. 275–83.
[17] Marsavina L, Sadowski T, Knec M. Crack propagation paths in four point bend aluminium–PMMA specimens. Eng Fract Mech 2013;108:139–51.
[18] Seed GM, Nowell D. Use of the distributed dislocations method to determine the T-stress. Fatigue Fract Eng Mater Struct 1994;17(5):605–18.
[19] Ayatollahi MR, Aliha MRM. Analysis of a new specimen for mixed mode fracture tests on brittle materials. Eng Fract Mech 2009;76:1563–73.
[20] Arcan M, Hashin Z, Voloshin A. A method to produce uniform plane-stress states with applications to fiber-reinforced materials. Exp Mech 1978;28:141–6.
[21] Richard HA, Benitz K. A loading device for the creation of mixed mode in fracture mechanics. Int J Fract 1983;22:55–8.
[22] Sander M, Richard HA. Experimental and numerical investigations on the influence of the loading direction on the fatigue crack growth. Int J Fatigue 2006;28(5):583–91.
[23] Biner SB. Fatigue crack growth studies under mixed-mode loading. Int J Fatigue 2001;23:259–63.
[24] Sharanaprabhu CM, Kudari SK, Iaeng M. Study on mixed mode crack-tip plastic zones in CTS specimen. In: Proceedings of the world congress on engineering, vol. II, July 2–4, 2008, London, UK.
[25] Liu Q, Qiu J, Ge S, Guo W. A finite element modeling and analysis of CTS specimen for three-dimensional I-II mixed mode fracture. In: Second international conference on information and computing science. http://dx.doi.org/10.1109/ICIC.2009.402.
[26] Jiang H, Gao X, Srivatsan TS. Predicting the influence of overload and loading mode on fatigue crack growth: a numerical approach using irreversible cohesive elements. Finite Elem Anal Des 2009;45:675–85.
[27] Kim CS, Chung KW. A study on fatigue crack propagation of rail steel under constant and mixed mode variable amplitude loadings. Int J Railw 2012;5(2):71–6.
[28] Patle V, Bhadauria SS, Abhishek J. Analysis of crack tip opening displacement under mixed mode fracture using fem technique. IOSR J Mech Civ Eng (IOSR-JMCE) 2012;3(5):27–34.
[29] Zhao J, Guo W. Three-parameter K-T–Tz characterization of the crack-tip fields in compact-tension-shear specimens. Eng Fract Mech 2012;92:72–88.
[30] Gouda PSS, Kodancha KG, Siddaramaiah D Jawali. Experimental and numerical investigations on fracture behavior of high silica glass/satin textile fiber reinforced hybrid polymer composites. Adv Mater Lett 2013;4(11):827–35.
[31] Demir O, İriç S, Ayhan AO, Lekesiz H. Investigation of mixed mode - I/II fracture problems - Part 1: computational and experimental analyses. Fract Struct Integr 2016;35:330–9. http://dx.doi.org/10.3221/IGF-ESIS.35.38.
[32] Demir O, Ayhan AO. Investigation of mixed mode-I/II fracture problems - Part 2: evaluation and development of mixed mode-I/II fracture criteria. Fract Struct Integr 2016;35:340–9. http://dx.doi.org/10.3221/IGF-ESIS.35.39.
[33] ANSYS. Theory manual version 12.0. Canonsburg (PA, USA): Ansys Inc; 2009.
[34] Ayhan AO, Nied HF. FRAC3D-finite element based software for 3-D and generalized plane strain fracture analysis. SRC technical report; 1998.
[35] Ayhan AO, Nied HF. Stress intensity factors for three-dimensional surface cracks using enriched elements. Int J Numer Method Eng 2002;54:899–921.

[36] Buchholz FG, Chergui A, Richard HA. Fracture analyses and experimental results of crack growth under general mixed mode loading conditions. Eng Fract Mech 2004;71:455–68.
[37] Ayhan AO. Mixed-mode stress intensity factors for deflected and inclined surface cracks in finite-thickness plates. Eng Fract Mech 2004;71(7–8):1059–79.
[38] Ayhan AO. Mixed-mode stress intensity factors for deflected and inclined corner cracks in finite-thickness plates. Int J Fatigue 2007;29(2):305–17.
[39] Ayhan AO. Finite element analysis of nonlinear deformation mechanisms in semiconductor packages Ph.D. dissertation. Lehigh University; 1999.
[40] Banks-Sills L, Arcan M, Bortman Y. A mixed mode fracture specimen for mode II dominant deformation. Eng Fract Mech 1984;20(1):145–57.
[41] Greer JM, Dorman SG, Hammond MJ. Some comments on the Arcan mixed-mode (I/II) test specimen. Eng Fract Mech 2011;78(9):2088–94.
[42] Gurubaran P, Afendi M, Kanasan N, Haftirman I, Tasyrif M, Basaruddin KS. Mixed mode loading fracture toughness of Arcan adhesive joint: effect of surface roughness. In: AIP conference proceedings. AIP Publishing LLC; 2016.
[43] ASTM International E399-12. Standard test method for linear-elastic plane-strain fracture toughness KIc of metallic materials; 2013.
[44] DataFit 9. Oakdale (PA): Oakdale Engineering; 2015 [15071].